

1 Introduction

The origin of fermion masses and mixings is one of most important issues in particle physics. Unfortunately, these parameters are inputs in the well-tested Standard Model (SM). All one can do is to measure them as accurately as possible and hope that in the future a more fundamental theory will actually be able to predict their values.

Fermion masses are possibly related to the electroweak symmetry breaking mechanism, which is not known at the moment. In the simplest model, a scalar electroweak doublet in an *ad hoc* quartic potential is responsible for the symmetry breaking, leaving a scalar physical boson, the Higgs boson ($J^{PC} = 0^{++}$), as a remnant. Favorite extensions of the SM, like the minimal supersymmetric standard model (MSSM), also predict the existence of a heavy pseudoscalar boson ($J^{PC} = 0^{-+}$), in addition to a light scalar boson. Another possibility is that the electroweak symmetry breaking is triggered by some new strong interactions, and in this case the lightest boson could be a pseudoscalar, like a pion [1]. Therefore, it is very important to distinguish between these two cases. This can be achieved by studying the parity properties of the scalar particle, once it is found. The general framework for performing this study in the decay of the Higgs into fermion or gauge boson pairs was developed in [2] and applied to Higgs production via Higgsstrahlung $e^+e^- \rightarrow ZH$ in [3].

Possibly the most direct way to measure the CP properties of the Higgs boson is in the environment of a photon-photon collider, by setting the polarization of the photon in order to select different CP states [4].

Details of the ZHH couplings can also be measured in a model independent way by studying the threshold behaviour and the angular distribution of the Higgsstrahlung process. In particular, the spin and parity assignments of the Higgs boson can be determined [5].

At future hadron machines, like the CERN Large Hadron Collider (LHC), weak gauge boson fusion can provide an efficient way to measure the CP properties of the HWW coupling by analysing the azimuthal angle distribution of the two outgoing forward tagging

jets [6].

The coupling of the Higgs boson to top quarks can also be used as a measure of the CP properties of the higgs boson in the processes $pp \rightarrow t\bar{t}h$ at the LHC [7] and $e^+e^- \rightarrow t\bar{t}H$ at a future Linear Collider [8]. Prospects of measuring the parity of the Higgs boson have also been analysed in $\mu^+\mu^-$ machines [9].

In this paper we concentrate on the determination of the (pseudo)scalar-tau-tau coupling at a Linear Collider with a center-of-mass energy of $\sqrt{s} = 500$ GeV and accumulated luminosity of 1 ab^{-1} , based on the Tesla proposal [10]. We wil assume that this particle has already been discovered at the Large Hadron Collider but a detailed study of its couplings is missing.

Contrary to previous works [11, 12], where only Higgsstrahlung and Higgs radiation off a heavy fermion leg were considered, we take into account all relevant contributions to the process $e^+e^- \rightarrow \tau^+\tau^-\nu\bar{\nu}$, where ν can be an electron, muon or tau neutrino. In particular, weak gauge boson fusion is the dominant contribution to Higgs production for $M_H < 180$ GeV at $\sqrt{s} \geq 500$ GeV.

In extensions of the SM with extra scalars and pseudoscalars, the lightest spin-0 particle can be an admixture of states without a definite parity [12]. Hence, we parametrize the general $H\tau\tau$ coupling as:

$$\frac{m_\tau}{v}(a + i\gamma_5 b) \quad (1)$$

where $v = 246$ GeV and $a = 1, b = 0$ in the Standard Model. We will present results considering a and b as independent parameters and also for the cases of fixed $a = 1$, free b and fixed $b = 0$, free a . We'll see that there is a region of insensitivity around circles of $\sqrt{a^2 + b^2} = 1$ in the $a - b$ plane.

Without considering τ decays, we are only sensitive to terms proportional to a , which comes from the interference with non-Higgs contributions, and a^2 and b^2 from pure Higgs contributions. Therefore, even at the τ level we can search for deviations from the Standard Model prediction which could arise, for instance, in supersymmetric models.

The analysis of τ decays permits to study some P-odd correlations which isolates the

effects of the b term and hence can distinguish between a scalar and pseudoscalar (or a CP-violating mixture) nature of the Higgs-tau-tau coupling. This will be the subject of a forthcoming publication.

2 Monte-Carlo simulation

We generate all possible contributions to the process $e^+e^- \rightarrow \tau^+\tau^-\nu\bar{\nu}$, where ν can be either an electron, muon or tau neutrino. The following contributions are computed:

- $e^+e^- \rightarrow \tau^+\tau^-\nu_e\bar{\nu}_e$: there are 21 Feynman diagrams that contribute to this process (see Fig. 1), of which only Diag. 10 (W-fusion) and Diag. 17 (Higgssthralung) are signal contributions;
- $e^+e^- \rightarrow \tau^+\tau^-\nu_\mu\bar{\nu}_\mu$: there are 11 Feynman diagrams in this case (see Fig. 2), of which only Diag. 8 (Higgssthralung) contributes to the signal;
- $e^+e^- \rightarrow \tau^+\tau^-\nu_\tau\bar{\nu}_\tau$: there are 20 Feynman diagrams in this case (see Fig. 3), of which only Diag. 17 (Higgssthralung) contributes to the signal.

The cross sections for these three contributions, with $m_H = 100$ GeV for illustration, are respectively $\sigma_{\nu_\tau} = 2.81 \times 10^{-2}$ pb, $\sigma_{\nu_\mu} = 1.25 \times 10^{-2}$ pb, and $\sigma_{\nu_e} = 0.109$ pb. As expected, σ_{ν_e} is dominant due to the fusion diagram.

In Fig. 4 we show the dependence of the total cross section $e^+e^- \rightarrow \tau^+\tau^-\nu\bar{\nu}$, summed over the three neutrino species, on the parameters $\Delta a = a - 1$ and b . The dependence in b is symmetric since only terms proportional to b^2 contribute to the cross section. On the other hand, the dependence on Δa is asymmetric due to interference with standard model processes, which leads to the presence of linear terms in Δa . Our goal is to see how sensitive the experiments performed at the next generation of e^+e^- colliders will be in the determination of these parameters.

3 Analysis

3.1 Experimental Aspects

To proceed with the analysis of the $e^+e^- \rightarrow \tau^+\tau^-\nu\bar{\nu}$ process one needs to have the final state topology as well as the τ 's momenta reconstructed.

For the generated data sample of the $e^+e^- \rightarrow \tau^+\tau^-\nu\bar{\nu}$ process we assume that tau-lepton pairs in the final state can be reconstructed in the experiment by using τ decays into π and ρ . The $\tau \rightarrow \pi\nu$ and $\tau \rightarrow \rho\nu$ decay channels are the two most important and together provide about 13% of the total branching ratio of τ pairs. As it was shown in the LEP/SLC studies, other channels, such as $\tau^\pm \rightarrow \pi^-\pi^+\pi^\pm\nu$, $\tau^\pm \rightarrow \pi^0\pi^0\pi^\pm\nu$, as well as leptonic tau decay modes, can be included increasing the experimental data sample to 82% .

There are several methods which can be used to reconstruct the final τ pair topology [13]. Recently, a new method [14] was proposed, which allows one to have a high reconstruction efficiency in the $\tau^\pm \rightarrow \rho^\pm\bar{\nu}_\tau(\nu_\tau)$, $\rho^\pm \rightarrow \pi^\pm\pi^0$ decay chain. This method was used to study the Higgs boson's parity using $\tau \rightarrow \rho\nu$ [15].

The results of the LEP experiments [16] show that the τ reconstruction efficiency varies from 51% to 80% . Based on the above results we adopt the moderate τ -pair reconstruction efficiency $\varepsilon_{\tau\tau} = 50\%$.

Another important aspect is the assumption about the detector performance and possible sources of the systematic uncertainties. We include the anticipated systematic errors of 0.5% in the luminosity measurement, 1% in the acceptance determination, 1% in the branching ratios, and 1% in the background subtraction, and assume the Gaussian nature of the systematics. To place bounds on the $H\tau^+\tau^-$ couplings, we use a standard χ^2 -criterion to analyse the events. We found that the most strict bounds are achieved by dividing the distribution event samples into 10 bins.

As for the possible contribution from background processes, like $e^+e^- \rightarrow e^+e^-ZZ \rightarrow e^+e^-\tau^+\tau^-\nu\bar{\nu}$ (with e -pair lost), $e^+e^- \rightarrow \nu\bar{\nu}W^+W^- \rightarrow \nu\bar{\nu}\tau^+\tau^-\nu\bar{\nu}$, $e^+e^- \rightarrow ZZZ \rightarrow \tau^+\tau^-\nu\bar{\nu}\nu\bar{\nu}$ etc., the cross-sections of these processes are either small, or they can be significantly suppressed without much difficulties, as it was shown in the analogous study

for the process $e^+e^- \rightarrow \nu\bar{\nu}H \rightarrow \nu\bar{\nu}b\bar{b}$ [17].

3.2 Kinematical Distributions

We analysed various distributions in order to determine which one is most sensitive to new physics: in the T correlation, defined by $T = \frac{1}{(\sqrt{s})^3} \vec{p}_{el} \cdot (\vec{p}_{\tau_1} \times \vec{p}_{\tau_2})$, the τ momentum $|\vec{p}_\tau|$, the angle between τ and the beam $\cos\theta_{e\tau}$ and the τ pair invariant mass $M_{\tau^+\tau^-}$. They are shown in Fig. 5 for the Standard Model, all plotted with 10 bins for illustration purposes.

In Fig.6, we illustrate the difference in the Higgs contributions in these distributions for the standard model ($a = 1, b = 0$) and ($a = 0.5, b = 0.5$). We see that the shapes are very similar, as expected, but the levels can be noticeable different.

In order to find the level of sensitivity, we show in Fig.7 the quantity $\frac{(\sigma_i^{New} - \sigma_i^{SM})}{\Delta\sigma_i^{exp}}$ for each bin of the distributions, where σ^{New} is the cross-section with a and/or b different from their SM values. In this figure, we used $a = 1, b = 0.5$ as an example of new physics. A luminosity $\int \mathcal{L} dt = 1 \text{ ab}^{-1}$ was used. We would like to stress again that including the contribution from W boson fusion enhances significantly the sensitivity and the result seems to be not so pessimistic as pointed out in [11].

In order to determine the sensitivity regions in the $a - b$ plane that can be probed in the next generation of linear colliders, we used the standard χ^2 method where the experimental error $\Delta\sigma_i^{exp}$ is given by:

$$\Delta\sigma_i^{exp} = \sigma_i^{SM} \sqrt{\delta_{syst}^2 + \delta_{stat}^2} \quad (2)$$

where

$$\delta_{stat} = \frac{1}{\sqrt{\sigma_i^{SM} \varepsilon_{\tau\tau} \int \mathcal{L} dt}} \quad (3)$$

and δ_{syst}^2 is the sum in quadrature of the systematic uncertainties mentioned above.

In order to understand the relative contributions for each class of diagrammas in Figs. 1–3, we show in Fig.8 the individual contributions from electron neutrinos, muon neutrinos

and tau neutrinos channels. As expected, electron neutrinos dominate due to the weak gauge boson fusion contribution.

4 Results

In order to determine the sensitive region in the parameter space, we decided to use the $\cos \theta_{e\tau}$ distribution, since the τ direction is possibly the easiest observable to be reconstructed from data. We also found that using 10 bins in the analysis optimizes the results.

We investigated the effects of the luminosity and the results are presented in Fig. 9, where the sensitivity regions for $\int \mathcal{L} dt = 100 \text{ fb}^{-1}$, 1 ab^{-1} and 10 ab^{-1} are shown. We can easily see what can be gained from an increase of luminosity at TESLA.

In Fig. 10, we show our final results for a Tesla-like environment, with luminosity of 1 ab^{-1} and center-of-mass energy of 500 GeV and for $M_H = 100 \text{ GeV}$. We adopted a 50 % τ -pair reconstruction efficiency and a systematic error of $\simeq 2\%$, in accordance with Tesla Design Report [10]. The allowed region for independent Δa and b parameters at 95% confidence level is the area between the solid circles. The horizontal band with long-dashed lines is the allowed region for the b parameter keeping $a = 1$. The two vertical bands with short-dashed lines are the the allowed region for the Δa parameter keeping $b = 0$ (of course only the right band containing the SM point is physical).

The bounds that can be obtained at 95% confidence level are:

1. The case of two independent parameters:

$$(0.70)^2 \leq (\Delta a + 1)^2 + b^2 \leq (1.23)^2 .$$

2. The case of $b = 0$ and free Δa :

$$-0.30 \leq \Delta a \leq 0.23 .$$

3. The case of $\Delta a = 1$ and free b :

$$-0.7 \leq b \leq 0.7 .$$

These results can be easily scaled for moderate variations in the Higgs boson mass around 100 GeV by multiplying the bounds by a factor $(M_H/100 \text{ GeV})^2$.

5 Conclusions

We have performed a complete analysis of the sensitivity to new $h\tau\tau$ couplings from the process $e^+e^- \rightarrow \tau^+\tau^-\nu\bar{\nu}$ at the next generation of linear colliders. These new couplings are predicted by many extensions of the Standard Model. We showed that forthcoming experiments will be able to probe deviations of $H\tau\tau$ coupling. For a Tesla-like environment, we are able to constrain the couplings in the region $(0.70)^2 \leq (\Delta a + 1)^2 + b^2 \leq (1.23)^2$ for independent a and b parameters. In order to disentangle the individual contributions of the parameters a and b , and to determine the CP nature of the Higgs boson, further analysis of τ decay products is needed. This will be the subject of a separate publication.

Acknowledgments

The work of A. Likhoded was partially funded by a Fapesp grant 2001/06391-4. The work of A. Chalov is partially supported by the Russian Foundation for Basic Research, grants 99-02-16558 and 00-15-96645, Russian Education Ministry, grant RF E00-33-062, and CRDF grant MO-011-0. R. Rosenfeld would like to thank Fapesp and CNPq for partial financial support. We would like to thank Claudio Dib for useful comments.

References

- [1] For a recent review, see C. T. Hill and E. H. Simmons, [hep-ph/0203079](#) and references therein.
- [2] J. R. Dell'Aquila and C. A. Nelson, Nucl. Phys. B **320** (1989) 61 and Nucl. Phys. B **320** (1989) 86.

- [3] B. K. Bullock, K. Hagiwara and Alan D. Martin, Phys. Lett. B **273** (1991) 501; Nucl. Phys. B **395** (1993) 499.
- [4] B. Grzadkowski and J. F. Gunion, Phys. Lett. B **294** (1992) 361; M. Krämer, J. Kühn, M. L. Stong and P. M. Zerwas, Zeit. Phys. C **64** (1994) 21; J. F. Gunion and J. G. Kelly, Phys. Lett. B **333** (1994) 110.
- [5] K. Hagiwara and M. L. Stong Zeit. Phys. C **62** (1994) 99; D. J. Miller, S. Y. Choi, B. Eberle, M. M. Muhlleitner and P. M. Zerwas, Phys. Lett. B **505** (2001) 149; V. Barger, K. Cheung, A. Djouadi, B.A. Kniehl and P. M. Zerwas, Phys. Rev. D **49** (1994) 79; K. Hagiwara, S. Ishihara, J. Kamoshita and B. A. Kniehl, Eur. Phys. J. C**14** (2000) 457; T. Han and J. Jiang, Phys. Rev. D **63** (2001) 096007.
- [6] T. Plehn, D. Rainwater and D. Zeppenfeld, Phys. Rev. Lett. **88** (2002) 051801.
- [7] J. F. Gunion and J. Pliszka, Phys. Lett. B **444** (1998) 136.
- [8] J. F. Gunion, B. Grzadkowski, X.-G. He, Phys. Rev. Lett. **77** (1996) 5172.
- [9] D. Atwood and A. Soni, Phys. Rev. D **52** (1995) 6271; V. D. Barger, M. S. Berger, J. F. Gunion and T. Han, Phys. Rep. **286** (1997) 1; V. D. Barger, T. Han and C.-G. Zhou, Phys. Lett. B **480** (2000) 140; B. Grzadkowski, J. F. Gunion and J. Pliszka, Nucl. Phys. B **583** (2000) 49.
- [10] *Physics at an e^+e^- linear collider*, Tesla Design Report, part 3, [hep-ph/0106315](https://arxiv.org/abs/hep-ph/0106315) .
- [11] G. Bower, talk presented at the *Linear Collider Workshop*, Chicago, January 7-9, 2002.
- [12] B. Grzadkowski and J. F. Gunion, Phys. Lett. B **350** (1995) 218; B. Grzadkowski, J. F. Gunion and J. Kalinowski, Phys. Rev. D **60** (1999) 075011.
- [13] M. Kramer, J. H. Kühn, M. L. Stong, and P. M. Zerwas, *Z. Phys. C***64** (1994) 21; T. Pierzchala, E. Richter-Was, Z. Was, and M. Worek, *Acta Phys. Polon. B***32** (2001) 1277.

- [14] Z. Was and M. Worek, [hep-ph/0202007](#).
- [15] G.R.Bower et al., [hep-ph/0204292](#), 2002.
- [16] See, *e.g.*, DELPHI Collaboration, *Nucl. Phys.* **B98** (Proc. Suppl.), (2001), 191.
- [17] K. Desch and N. Meyer, *LC Notes*, LC-PHSM-2001-025, 2001.

Figure captions

Figure 1: Feynman diagrams for the process $e^+e^- \rightarrow \tau^+\tau^-\nu_e\bar{\nu}_e$.

Figure 2: Feynman diagrams for the process $e^+e^- \rightarrow \tau^+\tau^-\nu_\mu\bar{\nu}_\mu$.

Figure 3: Feynman diagrams for the process $e^+e^- \rightarrow \tau^+\tau^-\nu_\tau\bar{\nu}_\tau$.

Figure 4: The total cross section $e^+e^- \rightarrow \tau^+\tau^-\nu\bar{\nu}$ dependence on Δa (solid line) and b (dashed line).

Figure 5: Distributions in T correlation, the τ momentum $|\vec{p}_\tau|$, the angle between τ and the beam, $\cos\theta_{e\tau}$ and the τ pair invariant mass, $M_{\tau^+\tau^-}$.

Figure 6: Contribution of Higgs diagrams to the differential distributions in the $e^+e^- \rightarrow \tau^+\tau^-\nu\bar{\nu}$ process for standard model ($a = 1, b = 0$, black dots) and $a = 0.5, b = 0.5$ (crossed dots).

Figure 7: Sensitivity functions $\frac{\sigma^{New} - \sigma^{SM}}{\Delta\sigma^{exp}}$ for each bin of the distributions, where as an example we took $a = 1, b = 0.5$ for new physics.

Figure 8: Relative contributions to the sensitivity functions of electron neutrino (black dots), muon neutrino (rectangular crossed dots), and tau neutrino (crossed round dots) channels.

Figure 9: Allowed regions for $\mathcal{L} = 100 \text{ fb}^{-1}$ (the domain inside the solid circle – there is no inner circle for this case), 1 ab^{-1} (domain confined by short-dashed contours), and 10 ab^{-1} (long-dashed contours).

Figure 10: The allowed region for independent Δa and b parameters at 95% confidence level is the area between the solid circles. The horizontal band with long-dashed lines is the allowed region for the b parameter keeping $a = 1$. The two vertical bands with short-dashed lines are the the allowed region for the Δa parameter keeping $b = 0$

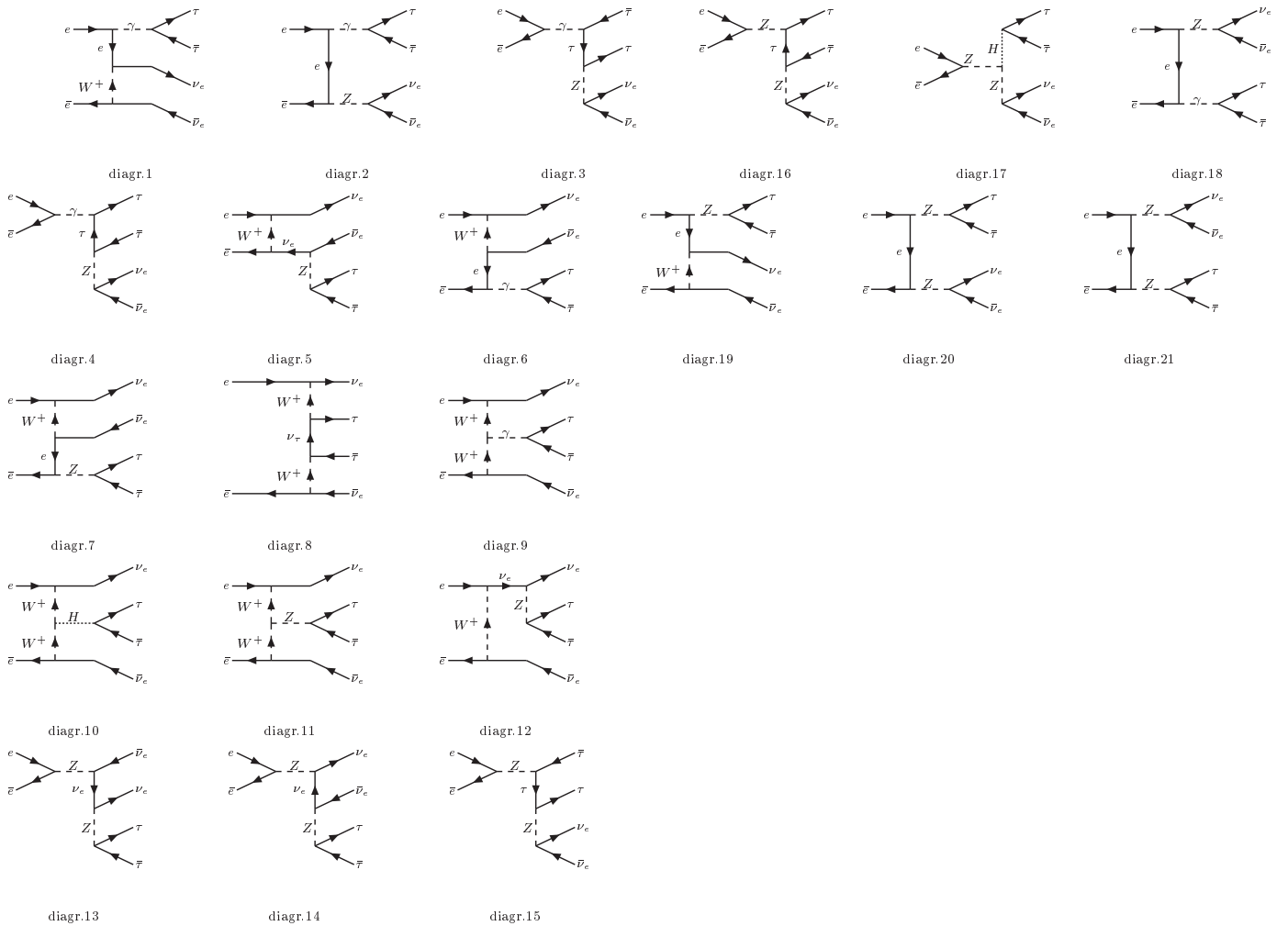


Figure 1:

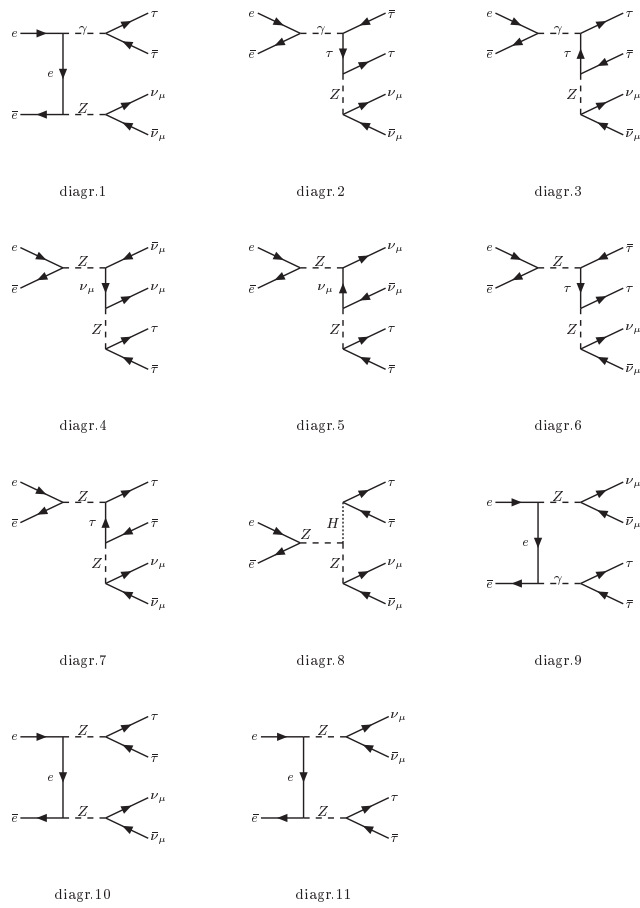


Figure 2:

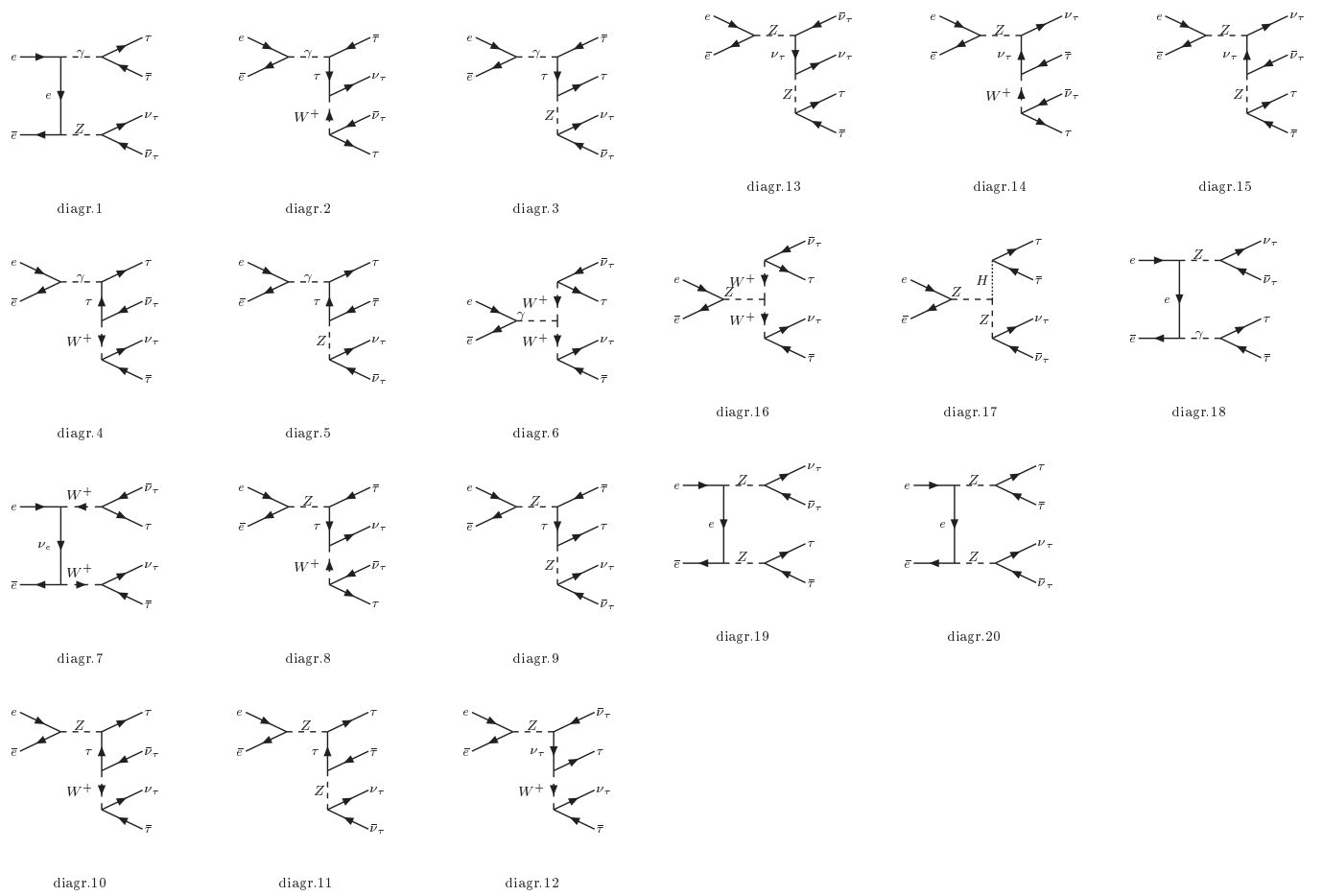


Figure 3:

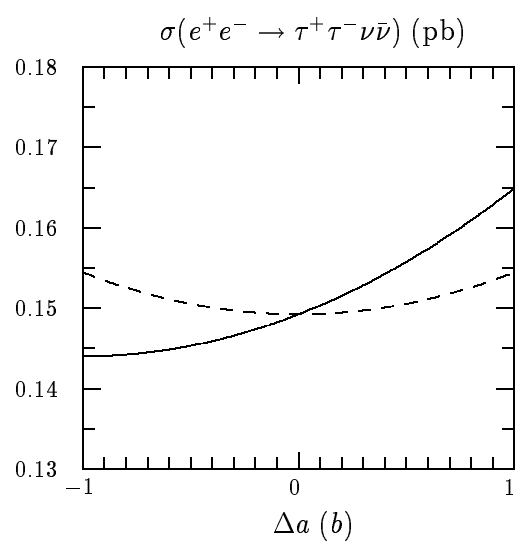


Figure 4:

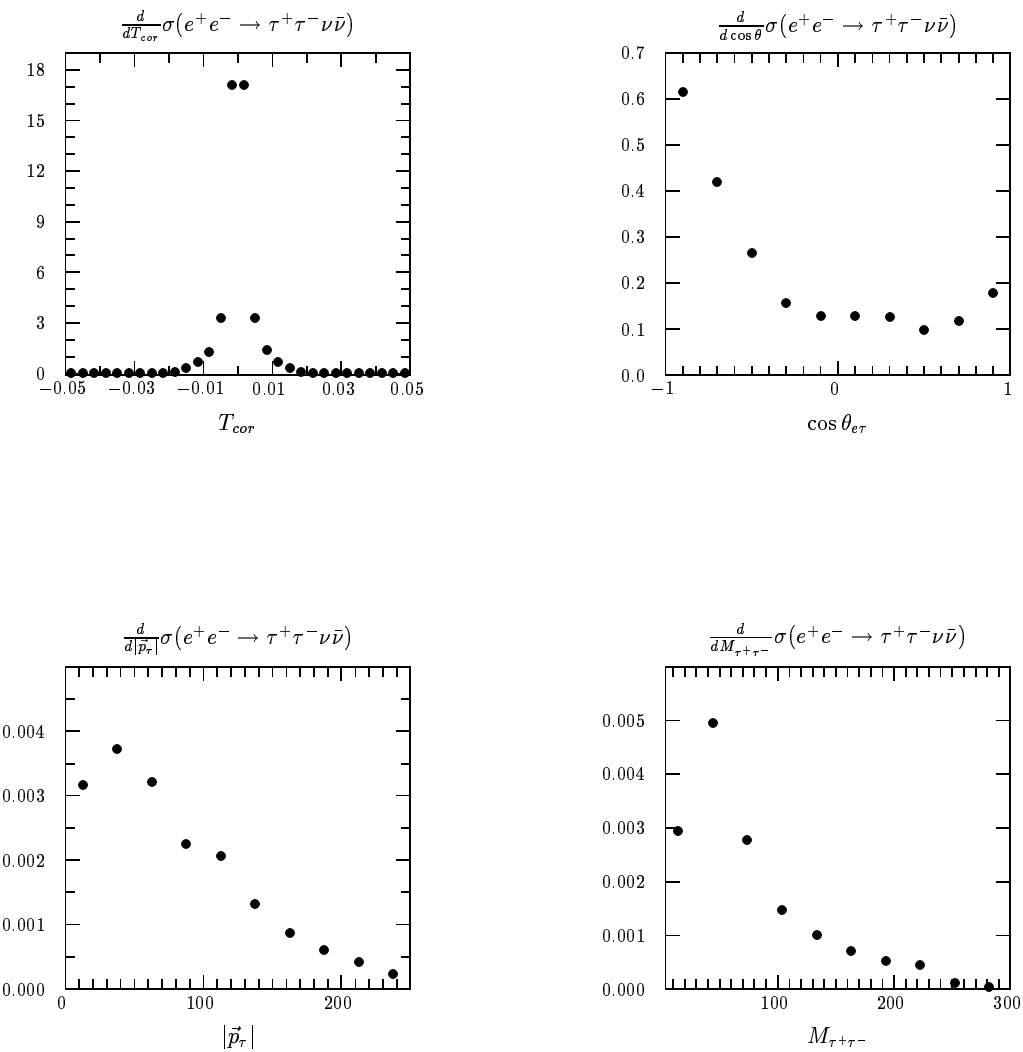


Figure 5:

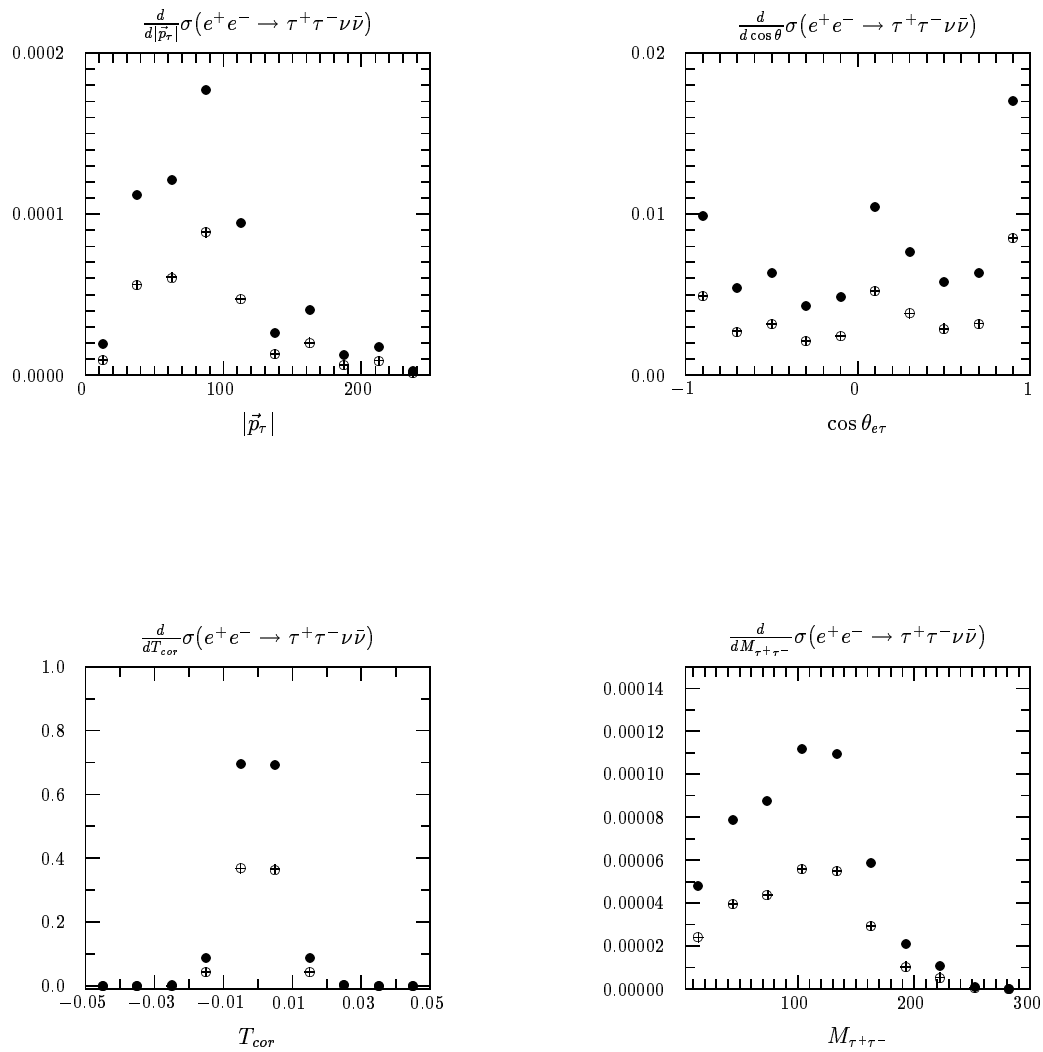


Figure 6:

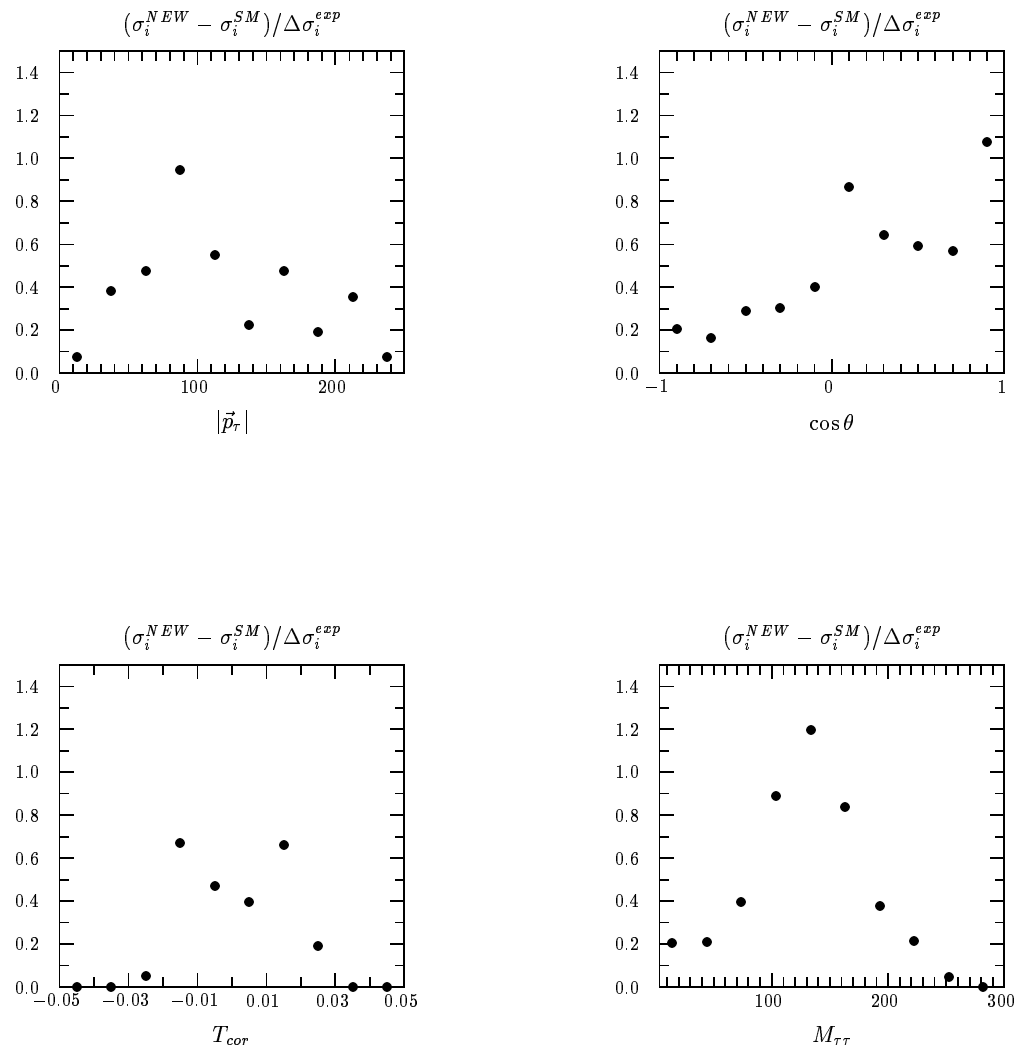


Figure 7:

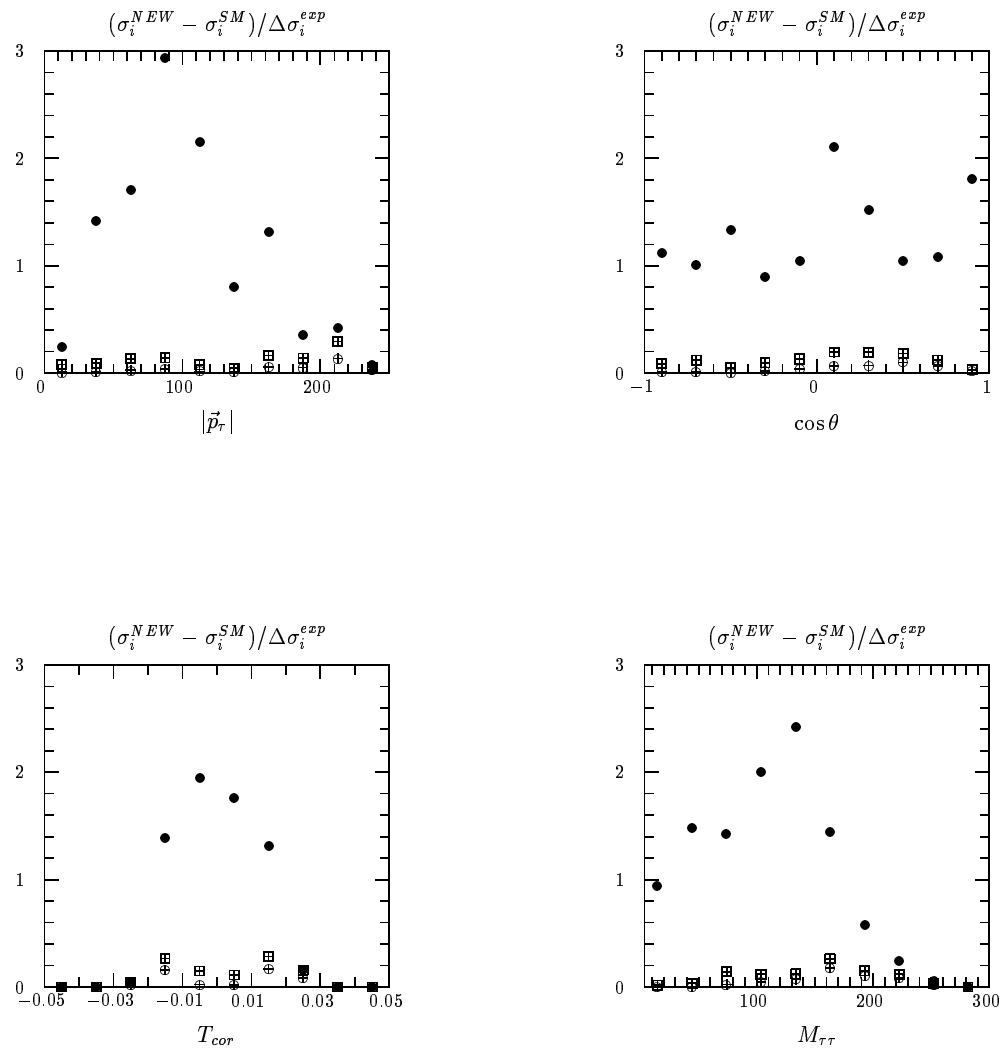


Figure 8:

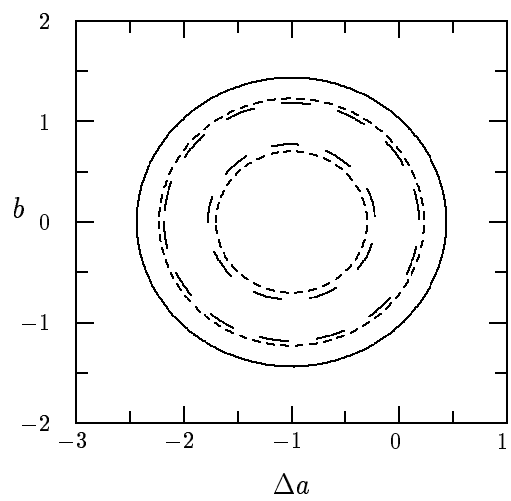


Figure 9:

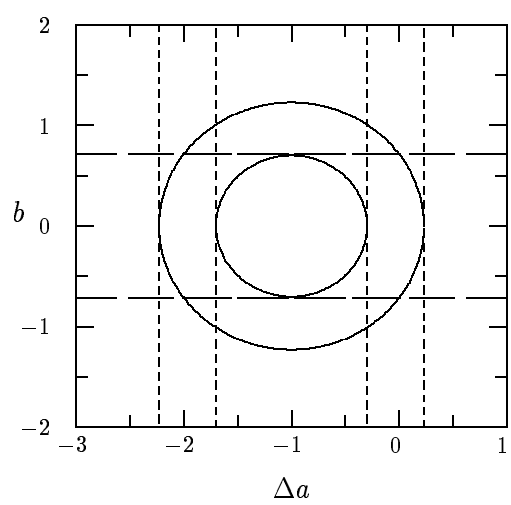
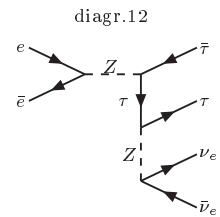
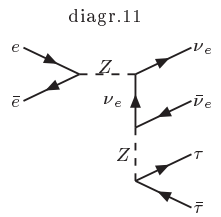
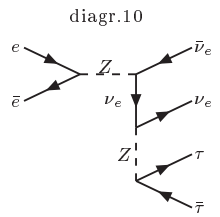
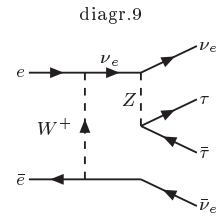
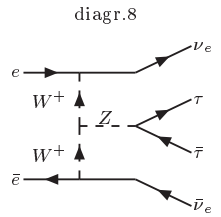
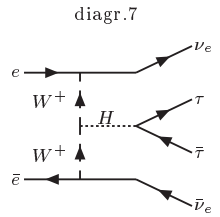
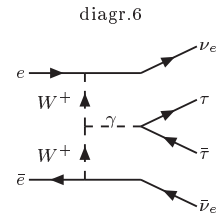
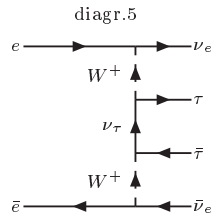
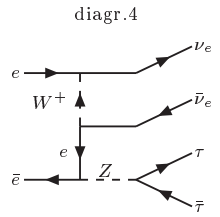
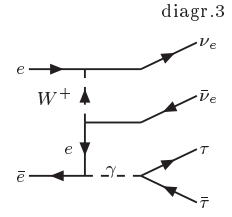
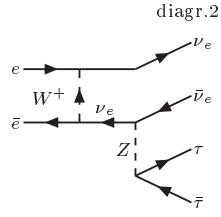
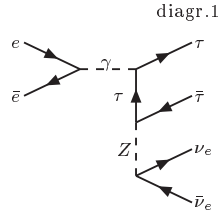
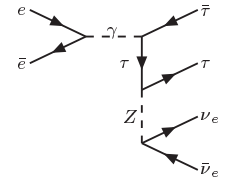
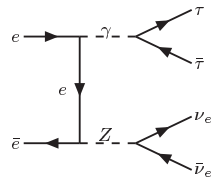
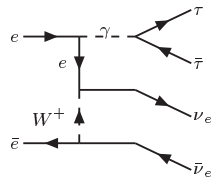


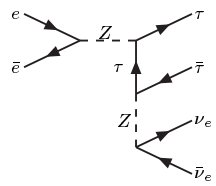
Figure 10:



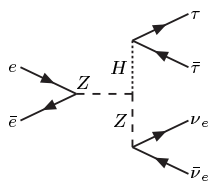
diagr.13

diagr.14

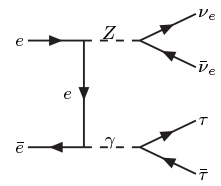
diagr.15



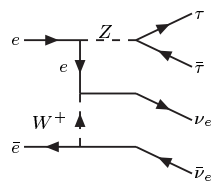
diagr.16



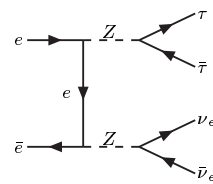
diagr.17



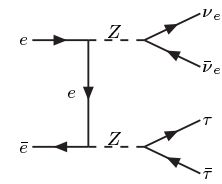
diagr.18



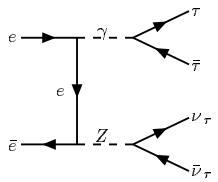
diagr.19



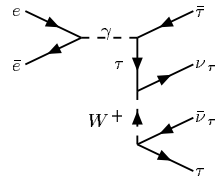
diagr.20



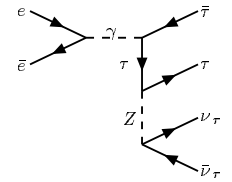
diagr.21



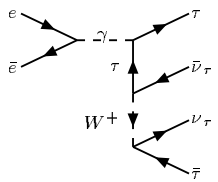
diagr.1



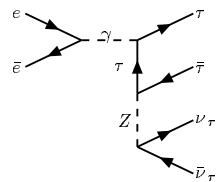
diagr.2



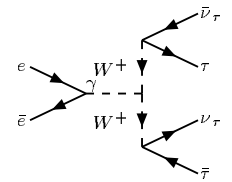
diagr.3



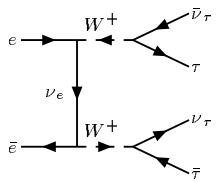
diagr.4



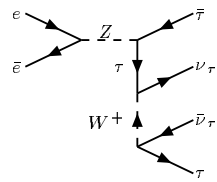
diagr.5



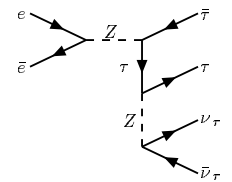
diagr.6



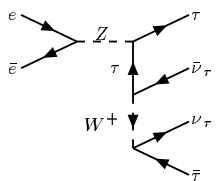
diagr.7



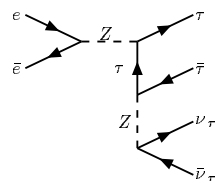
diagr.8



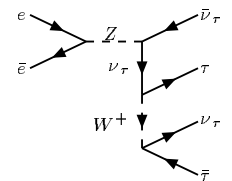
diagr.9



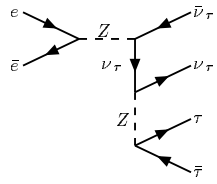
diagr.10



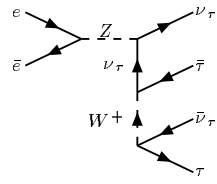
diagr.11



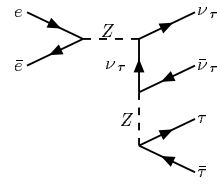
diagr.12



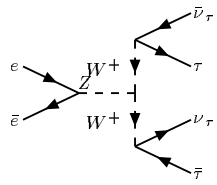
diagr.13



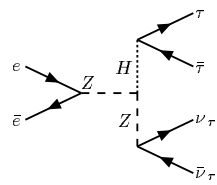
diagr.14



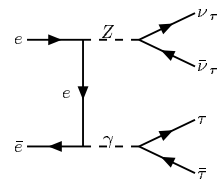
diagr.15



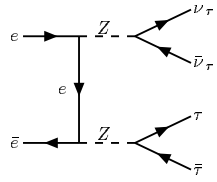
diagr.16



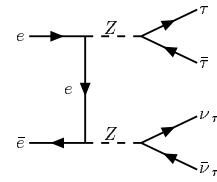
diagr.17



diagr.18



diagr.19



diagr.20